photolysed spot was 6.5 ± 3 μm in brain slices, as measured by caged fluorescein dextran (Fig. 1a, dextran BMNB-caged fluorescein, Molecular Probes). Moving the laser excitation horizontally or vertically so that the basal dendrite was more than 15–20 μm from the centre of laser excitation eliminated the EPSLP altogether ($n = 5$). Excitatory postsynaptic-like potentials evoked by glutamate uncaging at a rate of 1–2 min^{-1} remained stable over the time period tested (up to 40 min, $n = 9$). Blocking both AMPA and NMDA receptors with CNQX (10 μM) and AP5 (50–150 μM) eliminated the response during glutamate uncaging ($n = 4$).

Imaging techniques

Neurons were loaded with either CG1 (150–500 μM) or OGB-1 (200 μM) through the recording patch pipette and the basal dendritic tree including dendritic spines was imaged. For calcium imaging we used two experimental setups. Experiments using focal glutamate uncaging were performed on an MRC 600 confocal scan head (Bio-Rad) equipped with both an argon ion 488-nm laser (Ion Laser Technology) and a 880-nm two-photon laser (Innova 400 pumping a Mira 900, Coherent) mounted on an upright BX50WI Olympus microscope equipped with a 60× (Olympus 0.9 NA) water objective. Full images were obtained with a temporal resolution of 1 Hz and analysed using Analyse software (Mayo Foundation). Experiments using focal synaptic stimulation were performed using a modified confocal scan head (TCS 4D, Leika Microsystems) mounted on an upright BX50WI Olympus microscope equipped with a 40× (LUMPlanFl 40XW0.9IR, Olympus) water immersion objective. Data were obtained in the line scan mode with a temporal resolution of 4.5 ms and analysed with Igor software[8].

Modelling procedure

Computer simulations were performed using the compartmental modelling package NEURON[9] on a Pentium II PC under Windows NT. The modelling was performed on a reconstructed thick tufted layer 5 pyramidal cell. The neuron was reconstructed by A. Larkman as described[10]. The cell had 49 basal and 48 apical segments (branches) and a soma diameter of 18.5 μm. All the results shown are from inputs halfway along the first terminal basal segment. This had a length of 258 μm and a diameter of 0.84 μm after correction for shrinkage and after the spine collapse procedure. The integration method was CNEXP (Crank-Nicholson Exponential) with a time step of 25 μs. The temperature (Celsius parameter) was 25 °C. Passive parameters were modified from ref. 10 to match the decay time constants and amplitudes of modelled and experimental basal dendritic spikes.

In the model we used fast sodium, intermediate speed low voltage-activated, T-type (CaT) calcium, high voltage-activated calcium (CaH), NMDA and AMPA conductances. A modified Hodgkin–Huxley scheme was used for voltage-sensitive conductances, and the parameters for the voltage gated and synaptic conductances were based on published experimental data[11–17]. Some of the parameters were modified to allow better fit of the experimental results, and selected model parameters, including conductances (or densities), were varied manually to achieve a good match between the model and the experimental results. NEURON files can be obtained from G.M. (e-mail: gm@physiol.ox.ac.uk).

Received 2 November 1999; accepted 5 January 2000.

1. Larkman, A. U. Dendritic morphology of pyramidal neurons of the rat: Spine distribution. *J. Comp. Neurol.* **306,** 332–343 (1991).
2. Cash, S. & Yuste, R. Input summation by cultured pyramidal neurons is linear and position independent. *J. Neurosci.* **18,** 10–15 (1998).
3. Cash, S. & Yuste, R. Linear summation of excitatory inputs by CA1 pyramidal neurons. *Neuron* **22,** 383–94 (1999).
4. Schiller, J., Schiller, Y., Stuart, G. & Sakmann, B. Calcium action potentials in apical dendrites of neocortical pyramidal neurons in rat brain slices. *J. Physiol.* **505,** 605–616 (1997).
5. Bliss, T. V. P. & Collingridge, G. L. A synaptic model of memory: Long term potentiation in the hippocampus. *Nature* **361,** 31–39 (1993).
6. Schiller, J., Schiller, Y. & Clapham, D. E. NMDA receptors amplify calcium influx into dendritic spines during associative pre- and postsynaptic activation. *Nature Neurosci.* **1,** 114–118 (1998).
7. Stuart, G. J., Dodt, H. U. & Sakmann, B. Patch-clamp recordings from the soma and dendrites of neurons in brain slices using infrared video microscopy. *Pflug. Arch. Eur. J. Physiol.* **423,** 511–518 (1993).
8. Koester, H. J. & Sakmann, B. Calcium dynamics in single spines during coincident pre- and postsynaptic activity depend on relative timing of back-propagating action potentials and subthreshold excitatory postsynaptic potentials. *Proc. Natl Acad. Sci. USA* **95,** 9596–9601 (1998).
9. Hines, M. L. & Carnevale, N. T. The NEURON simulation environment. *Neural Comput.* **9,** 1179–1209 (1997).
10. Major, G., Larkman, A. U., Jonas, P., Sakmann, B. & Jack, J. J. B. Detailed passive cable models of whole-cell recorded CA3 pyramidal neurons in rat hippocampal slices. *J. Neurosci.* **14,** 4613–4638 (1994).
11. Ascher, P. & Nowak, L. The role of divalent cations in the *N*-methyl-D-aspartate responses of mouse central neurons in culture. *J. Physiol.* **399,** 247–266 (1988).
12. Hestrin, S., Nicoll, R. A., Perkel, D. J. & Sah, P. Analysis of excitatory synaptic action in pyramidal cells using whole-cell recording from rat hippocampal slices. *J. Physiol.* **422,** 203–225 (1990).
13. Brodin, L., Traven, H. G. C., Lansner, A., Wallen, P. & Ekeberg, O. Computer simulations of *N*-methyl-D-aspartate receptor-induced membrane properties in a neuron model. *J. Neurophysiol.* **66,** 473–484 (1991).
14. Brown, A. M., Schwindt, P. C. & Crill, W. E. Voltage dependence and activation kinetics of pharmacologically defined components of the high-threshold calcium current in rat neocortical neurons. *J. Neurophysiol.* **70,** 1530–1543 (1993).
15. Jonas, P., Major, G. & Sakmann, B. Quantal components of unitary EPSCs at the mossy fiber synapse on CA3 pyramidal cells of rat hippocampus. *J. Physiol.* **472,** 615–663 (1993).
16. Martina, M. & Jonas, P. Functional differences in Na^+ channel gating between fast-spiking interneurons and principal neurons of rat hippocampus. *J. Physiol.* **505,** 593–603 (1997).
17. Destexhe, A., Neubig, M., Ulrich, D. & Huguenard, J. Dendritic low-threshold calcium currents in thalamic relay cells. *J. Neurosci.* **18,** 3574–3588 (1998).

Acknowledgements

We thank. D. E. Clapham, F. Prendergast, B. Sakmann, W. Denk and D. Tank for assistance and support, A. Larkman for reconstructing the cell used in the simulations, and M. Hausser and G. Stuart for reading early versions of the manuscript. In addition we thank the Mayo Foundation, Leo & Frances Kogan endowment fund (J.S.), Wellcome Trust, Lucent Technologies and Marine Biological Laboratory (G.M.) for financial support.

Correspondence and requests for materials should be addressed to J.S. (e-mail: Jackie@tx.technion.ac.il).

The Ras-MAPK pathway is important for olfaction in *Caenorhabditis elegans*

Takaaki Hirotsu, Satoshi Saeki*†, Masayuki Yamamoto* & Yuichi Iino

Molecular Genetics Research Laboratory, The University of Tokyo, Tokyo 113-0033, Japan
** Department of Biophysics and Biochemistry, Graduate School of Science, The University of Tokyo, Tokyo 113-0033, Japan*

The Ras-MAPK (mitogen-activated protein kinase) signal transduction pathway is well known to control cellular proliferation and differentiation in response to extracellular signals, but its other functions are less understood. In *Caenorhabditis elegans* this pathway regulates several developmental events, such as vulval induction and progression of meiosis[1], but its function in the nervous system is unknown. Here we report that the Ras-MAPK pathway is involved in olfaction in this organism. Mutational inactivation and hyperactivation of this pathway impairs efficiency of chemotaxis to a set of odorants. Experiments in which *let-60 ras* was expressed using a heat-shock promoter and a cell-specific promoter show that a normal activity of LET-60 Ras is required in mature olfactory neurons. Application of the odorant isoamylalcohol to wild-type animals leads to the activation of MAP kinase in olfactory neurons within 10 seconds. This induction is dependent on the function of the nucleotide-gated channel TAX-2/TAX-4 and the voltage-activated calcium channel subunit UNC-2. These results suggest a dynamic regulatory role for the Ras-MAPK pathway in perception and transmission of sensory signals in olfactory neurons.

Chemotaxis to volatile chemoattractants in *C. elegans* is mediated primarily by two pairs of olfactory neurons, AWA and AWC (ref. 2). The gain-of-function (gf) mutant of *let-60 ras*, *let-60(n1046*gf*)*, shows a defect in chemotaxis to the AWC-sensed chemoattractants isomylalcohol (Fig. 1a, open bars), butanone and benzaldehyde (data not shown). It also shows a weak but statistically significant defect in chemotaxis to the AWA-sensed chemoattractant diacetyl (Fig. 1b, open bars). This oncogenic-type mutation in *let-60* is expected to lead to a reduced rate of conversion from the GTP-bound active form to the GDP-bound inactive form, and therefore hyperactivation, of the encoded Ras protein[3]. Defects in chemotaxis to AWA- and AWC-sensed odorants are also seen in the loss-of-function (lf) mutants *let-60(n2021)* and *lin-45(sy96)* and the

† Present address: Tokyo Research Laboratories, Kyowa Hakko Kogyo Co., Ltd, Machidashi, Tokyo 194-8533, Japan.

presumed null mutant *mek-2(n2678)*, where *lin-45* encodes a Raf MAPK kinase kinase and *mek-2* encodes a MAPK kinase, although the defects are very mild in some cases (Fig. 1a, b). These mutants also exhibit defects in chemotaxis to 2,4,5-trimethylthiazole, where AWA and AWC have overlapping functions[2] (Fig. 1c). It has previously been found that the *mek-2* mutants show poor chemotaxis to *Escherichia coli*[4], and our results are consistent with this observation. The defect of *let-60(gf)* in chemotaxis to isoamylalcohol is suppressed by loss-of-function mutations in the downstream genes. These include a loss-of-function mutation in the *ksr-1* gene encoding KSR (kinase suppressor of ras)[5,6] and weak loss-of-function mutations *mek-2(ku114)* and *mpk-1(n2521)*, where *mpk-1* encodes a MAP kinase (Fig. 1d). These results indicate that LET-60 Ras may be involved in chemotaxis to AWA- and AWC-sensed volatile chemoattractants and that the MAPK pathway functions downstream of LET-60 Ras. The defects in these mutants in chemotaxis to odorants are unlikely to be due to a general abnormality in locomotion, because these mutants can respond normally to the water-soluble attractant NaCl, which is sensed mainly by ASE neurons (Fig. 1e).

In vulval induction, SEM-5, an adaptor protein similar to mammalian Grb2, functions upstream of LET-60 Ras[7], and LIN-1, a transcription factor with partial similarity to mammalian Elk-1, is one of the target molecules of MAPK[8]. The *sem-5(n2019)* and *lin-1(e1777)* mutants show normal chemotaxis to both AWA- and AWC-sensed odorants (data not shown). Thus, these components are unlikely to be shared by the signalling cascade required for normal chemotaxis.

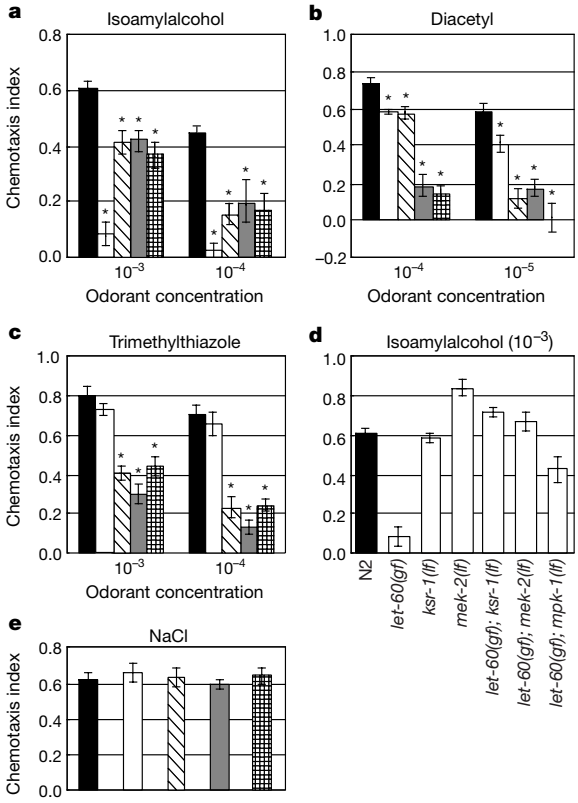

Figure 1 Chemotaxis of mutants affected in the Ras-MAPK pathway. **a**, Chemotaxis to isoamylalcohol, which is sensed mainly by AWC chemosensory neurons, of wild-type N2 (filled bars), *let-60(n1046*gf) (open bars), *let-60(n2021*lf) (hatched bars), *lin-45(sy96*lf) (stippled bars) and *mek-2(n2678*lf) (cross-hatched bars). The attractant dilutions used are indicated at the bottom. **b**, Chemotaxis to diacetyl, which is sensed mainly by AWA neurons, depicted as in **a**. **c**, Chemotaxis to 2,4,5-trimethylthiazole, sensed by AWA and AWC neurons, depicted as in **a**. **d**, Chemotaxis to isoamylalcohol at 10^{-3} dilution. Strains: wild-type N2, *let-60(n1046)*, *ksr-1(ku68)*, *mek-2(ku114)*, *let-60(n1046);ksr-1(ku68)*, *mek-2(ku114);let-60(n1046)* and *mpk-1(n2521);let-60(n1046)*. **e**, Chemotaxis to 100 mM sodium chloride. Bars are labelled as in **a**.

Because the *let-60(gf)* mutant shows a stronger defect in AWC-mediated chemotaxis, we determined whether there is any abnormality in AWC chemosensory neurons in mutant animals. The *gcy-10* promoter drives expression in the chemosensory neurons AWC and AWB and in the pharyngeal interneuron I1 (ref. 9). We visualized these neurons using the *gcy-10*::*GFP* marker. A pair of AWC cell bodies was clearly visible in N2 animals transgenic for *gcy-10*::*GFP*. Another pair of cell bodies, AWB, was also visible, although less bright, whereas I1 appeared very faint. AWC cell bodies were present normally in the *let-60(gf)* and *let-60(lf)* mutants (Fig. 2). No gross morphological abnormalities, such as the generation of new axon branches reported for *tax-2*, *tax-4* and several other mutants[10–12], were noticed in the axons or dendrites.

Given the chemotactic defect in the mutants, an important issue is whether the Ras-MAPK pathway is required for the development or function of differentiated cells. We therefore expressed *let-60* under the control of the heat-shock promoter *hsp16-2*. All the structures essential for chemotaxis differentiate during embryogenesis in *C. elegans* hermaphrodites. We first examined the effect of *let-60(gf)* expression from the *hsp*::*let-60(gf)* transgene in the wild-type background. Animals in which *let-60(gf)* was expressed during embryogenesis showed a normal response to isoamylalcohol and diacetyl (Fig. 3a). In contrast, chemotaxis to isoamylalcohol and to diacetyl decreased significantly when *let-60(gf)* was expressed in adults (Fig. 3b, c). These results indicate that the ectopic activation of Ras in fully differentiated cells may impair chemotaxis. Again, chemotaxis to NaCl was not affected in these animals (data not shown).

In reciprocal experiments, the expression of *let-60(+)* as a transgene in the *let-60(lf)* mutant during adulthood restored the response to isoamylalcohol and diacetyl significantly (Fig. 3d, e). Although the rescue was not complete, possibly because of unstable maintenance of the transgene as an extrachromosomal array or because of suboptimal expression levels, this result is consistent with chemotaxis requiring the normal function of *let-60* in differentiated cells.

To determine the site of action of *let-60*, we tested whether the expression of *let-60(gf)* in AWC chemosensory neurons is sufficient

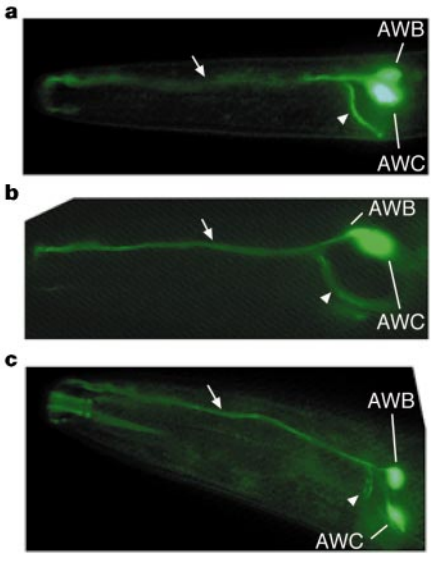

Figure 2 AWC neurons visualized with the *gcy-10*::*GFP* marker. Green fluorescent protein was seen in the AWC and AWB cell bodies (as indicated) in N2 (wild type) (**a**), *let-60(n1046*gf) mutant (**b**) and *let-60(n2021*lf) mutant (**c**). The dendrites (arrows) and axons (arrowheads) of these neurons were also visible and showed no gross morphological abnormalities. The anterior tip of the animal, where sensory cilia are located, is to the left in each panel.

to cause the defect in chemotaxis to AWC-sensed odorants. We placed *let-60(gf)* under the control of the *gcy-10* promoter, which acts in AWC, AWB and I1 neurons, and introduced it into wild-type animals. The transgenic lines showed a significant defect in chemotaxis to isoamylalcohol, which is sensed by AWC, but not to diacetyl, which is sensed by AWA (Fig. 3f). Similarly, *gcy-10*::*let-60(+)* restored the response of the *let-60(lf)* mutant to isoamylalcohol, but not to diacetyl (Fig. 3g). These results indicate that AWC neurons may be responsible for the chemotactic defects in both *let-60(gf)* and *let-60(lf)* mutants. Note that AWB chemosensory neurons, which also express *gcy-10*, sense volatile repellents and are dispensable for chemotaxis to volatile attractants[2,13], and that pharyngeal neurons, including I1, are mostly isolated from the somatic nervous system[14].

Our genetic analysis shows that the activity of the Ras-MAPK pathway in mature olfactory neurons is important for chemotaxis to AWC-sensed odorants. How, then, would the Ras-MAPK pathway be activated in olfactory neurons? To assess the activity of the Ras-MAPK pathway directly, we used a monoclonal antibody to activated (diphosphorylated) MAP kinase. AWC neurons were identified by co-staining with anti-GFP antibodies in the *gcy-10*::*GFP* transformants. Immunoreactivity against the anti-activated-MAPK antibody was observed in the AWC neurons, along with several other neurons including AWB, after 10 seconds of application of isoamylalcohol at 10^{-2} or 10^{-4} dilution (Fig. 4a, b). The most intense staining is observed in the cell bodies of these neurons. Axons and dendrites also show weak but consistent staining, whereas no staining was ever observed in the sensory cilia. Only a few animals showed staining in the AWC neurons without odorant stimulus (Fig. 4b). In the *let-60(gf)* mutant, many neurons in the head region including AWC show intense staining irrespective of odorant application. In contrast, no staining was observed in the *let-60(lf)* mutants even after odorant stimulus (Fig. 4a, b). These observations indicate that the immunoreactivity detected with this antibody is a true MAP kinase activated downstream of LET-60 Ras.

We further examined the involvement of possible upstream components in this response. In AWC neurons, olfactory signals received by seven-transmembrane receptors are thought to be transmitted through G protein to the cGMP pathway. Mutations in the *odr-3* gene encoding a G protein α-subunit and in the *tax-2* or

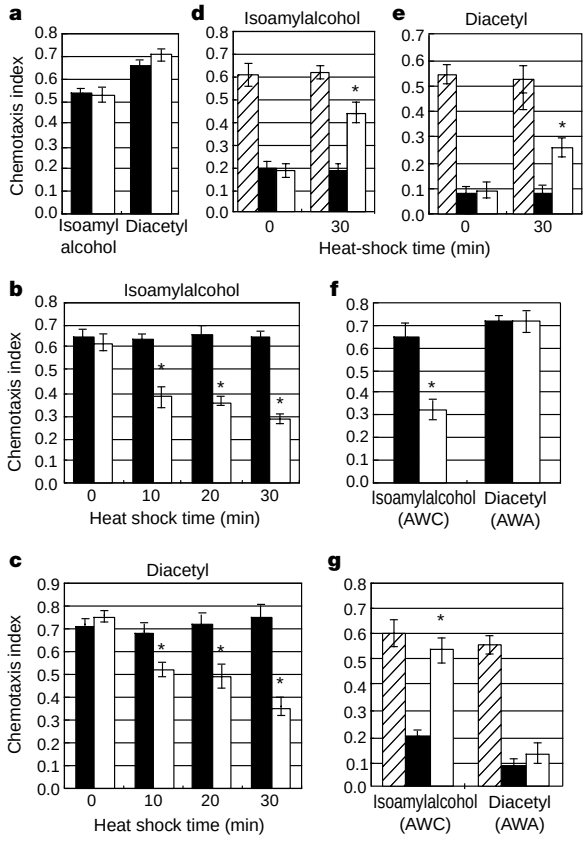

Figure 3 Temporally and spatially restricted expression of *let-60* affects chemotaxis to odorants. **a**–**c**, Heat shock was applied during embryogenesis (**a**) or adulthood (**b**, **c**) to wild-type animals transgenic for *hsp*::*let-60(gf)*, and chemotaxis to the indicated odorants was assayed (open bars). Control animals carried only pEF1α::GFP, the transformation marker (filled bars). **d**–**e**, The *let-60(n2021*lf*)* mutant carrying *hsp*::*let-60(+)* (open bars) or only pEF1α::GFP (filled bars) were subjected to heat shock as adults, and chemotaxis to isoamylalcohol (**d**) and diacetyl (**e**) was assayed. Hatched bars show wild-type animals carrying only pEF1α::GFP. **f**, Wild-type animals carrying *gcy-10*::*let-60(gf)* (open bars) and those carrying only pEF1α::GFP (filled bars) were assayed for chemotaxis to isoamylalcohol and diacetyl. **g**, The *let-60(n2021*lf*)* mutant carrying *gcy-10*::*let-60(+)* (open bars) and that carrying only pEF1α::GFP (filled bars) were assayed for chemotaxis to isoamylalcohol and diacetyl. Hatched bars show wild-type animals carrying only pEF1α::GFP. The dilution of isoamylalcohol was 10^{-3} (**a**, **b**, **f**) and 10^{-4} (**d**, **g**). The dilution of diacetyl was 10^{-4} (**a**, **c**, **f**) and 10^{-5} (**e**, **g**).

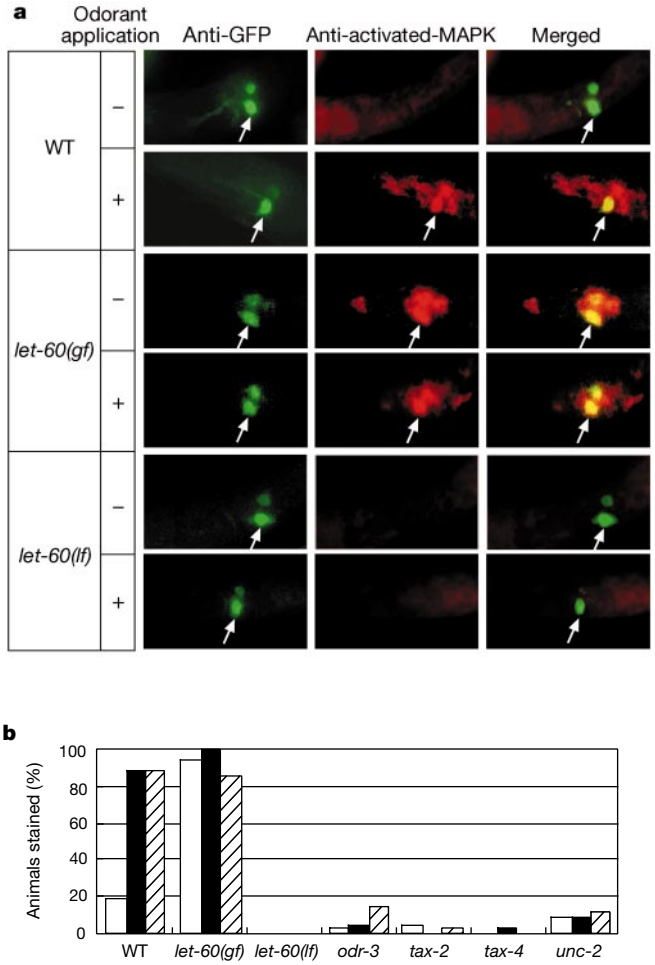

Figure 4 Activation of MAPK by odorant stimulus. **a**, Immunofluorescence images of anti-GFP staining (green), anti-activated-MAPK staining (red) and merged images (yellow indicates overlap). All figures show the left lateral views of the head regions of animals. '–', animals fixed without odorant application; '+', animals fixed 10 s after application of 10^{-2} dilution of isoamylalcohol. Arrows show AWC neurons. **b**, The proportion of animals showing staining with anti-activated-MAPK in AWC neurons. Animals were exposed for 10 s to isoamylalcohol at a concentration of 10^{-2} (filled bars) or 10^{-4} (hatched bars). Open bars show control experiments without application of the odorant. Strains: wild-type N2, *let-60(n1046*gf*)*, *let-60(n2021*lf*)*, *odr-3(n2150*lf*)*, *tax-2(p691*lf*)*, *tax-4*(*p678*lf*)*, *unc-2(e55*lf*)*. All were transgenic for *gcy-10*::*GFP*.

tax-4 genes encoding subunits of the cyclic nucleotide-gated cation channel cause defects in AWC-mediated chemotaxis[11,15,16]. Activation of MAP kinase by the application of isoamylalcohol is severely reduced or eliminated in any of these mutants (Fig. 4b). *unc-2* encodes a protein similar to the α_1-subunits of neuronal voltage-activated calcium channels[17]. Activation of the MAP kinase is also severely reduced in the *unc-2* mutant. These results suggest that odorant-induced neuronal activity is essential for the activation of the Ras-MAPK pathway.

This study provides the first evidence that the Ras-MAPK pathway functions in the nervous system of *C. elegans*. It is also the first observation, to our knowledge, that indicates a functional role for the Ras-MAPK pathway in olfactory neurons in any species. In *C. elegans*, as in vertebrates[18], olfactory signals are thought to be received by seven-transmembrane receptors and transmitted to the cGMP pathway, and to lead to cation influx through the TAX-2/TAX-4 channel in AWC olfactory neurons[19]. Our study has shown that the Ras-MAPK pathway functions downstream of these components.

Unexpectedly, MAPK was activated after only ten seconds of odorant stimulus in the chemosensory neuron cell bodies, which are nearly 100 μm away from the sensory cilia. This fast response, together with our observation that sensory cilia are devoid of activated MAPK, indicates that electrical activity may mediate the response. There is good evidence that *C. elegans* lack voltage-activated sodium channels, and that a depolarization-activated calcium current is essential for the maintenance of membrane depolarization[20,21]. The loss of the odorant-induced activation of MAPK in the *unc-2* mutant is, therefore, probably due to a failure to sustain electrical activity in the sensory neurons. In addition, calcium ions may be directly involved in the activation, possibly through a calcium-activated guanine nucleotide exchange factor similar to mammalian Ras-GRF (refs 22–24).

Our results show that both hyperactivation and inactivation of the pathway impairs chemotaxis. This suggests that Ras and the downstream MAPK should be properly activated in response to odorants and shut off in their absence, and that failure to do so leads to dysfunction of the sensory neurons. The pathway may, therefore, be directly involved in some aspect of synaptic transmission, such as regulation of synaptic vesicle supply. Otherwise it may have a regulatory role in chemosensation, such as adjustment of the dynamic range of the sensory system depending on the odorant concentration. The effects of MAPK could be through either transcriptional regulation or the direct phosphorylation of target molecules. Given the power of genetics in *C. elegans*, suppressor or enhancer screens should reveal downstream genes encoding targets or downstream effectors of MAPK. □

Methods

Chemotaxis assay

Chemotaxis assays for volatile odorants were performed on phosphate-buffered agar plates as described[2], except in the assay for diacetyl, for which MOPS-buffered agar plates were used[25]. Washed animals were placed ~3 cm from the point where the odorants had been spotted. Chemotaxis to NaCl was assayed essentially as described[26] on a phosphate-buffered assay plate in which a chemical gradient was formed for 15 h by an agar plug including 100 mM NaCl. Roughly 100 adult hermaphrodites grown at 20 °C were tested at 20 °C on each assay plate. All the strains used were viable and fertile as homozygotes and maintained as such, except for *mek-2(n2678)*, which were sterile as homozygotes. The *mek-2* allele was maintained as heterozygotes and only sterile progeny were counted in the chemotaxis assay. In Figs 1 and 3, each bar represents at least five independent assays. Error bars show s.e.m. and asterisks indicate that the values differ significantly ($P < 0.05$) from that of the control. Chemotaxis index = ((number of animals attracted to the chemoattractant) – (number of animals at the opposite end of the plate))/(total number of animals on the assay plate).

Germline transformation

Plasmids were injected into the gonad arms as described[27]. For visualization of the AWC neurons, the *gcy-10*::*GFP* construct (from D. Garbers) was injected with the plasmid pRF4, which contains a dominant allele of *rol-6*, as a transformation marker.

Heat shock experiments

Complementary DNAs corresponding to the wild-type *let-60* allele and to the *let-60(n1046*gf*)* allele (both from M. Han) were inserted into pPD49.78 (from A. Fire) which carries the heat-shock promoter *hsp16-2*. The resulting *hsp*::*let-60(gf)* was injected into N2 (wild type), and *hsp*::*let-60(+)* was injected into *let-60(n2021*lf*)* at a concentration of 50 μg ml^{-1} using pEF1α::GFP (from N. Hisamoto; 50 μg ml^{-1}) as a fluorescent transformation marker. This transformation marker did not affect chemotaxis or locomotion. For embryonic expression of the transgene, gravid hermaphrodites were collected and treated with alkaline hypochlorite to separate the embryos physically. Early embryos thus isolated were heat shocked at 30 °C for 8 h, and allowed to grow to adulthood at 20 °C, after which chemotaxis assay was conducted. For expression in adults, 10–30 min of heat shock at 33 °C was applied to adults suspended in buffer, and the chemotaxis assay was performed after recovery at 20 °C for 1 h. Only animals emitting green fluroescence under a fluorescence-equipped dissecting microscope (Olympus SZX12), which indicates the maintenance of the unstable extrachromosomal array, were counted in these assays.

Cell-specific expression

The promoter region (1.7 kb) of *gcy-10* was amplified by PCR from *C. elegans* genomic DNA and inserted into the pPD49.26 vector into which *let-60(+)* or *let-60(gf)* cDNA had been inserted. The *gcy-10*::*let-60* constructs were injected with pEF1α::GFP as a transformation marker at a concentration of 50 μg ml^{-1} each.

Immunohistochemistry

Animals were collected and kept in water for 3 h before odorant application. Excess water was removed after centrifugation and 50 μl of isoamylalcohol diluted in water was added. After 10 s, we added Bowin's fixative/Methanol/BME (40:40:1) and carried out immunofluorescence[28] using a fluorescent microscope (Zeiss Axioskop). Incubation with primary antibodies was at room temperature for 15 h, and secondary antibodies were incubated at room temperature for 2 h. The primary antibodies used were mouse anti-diphosphorylated-ERK1&2 monoclonal antibody (Sigma M8159)[29] at 1/800, and rabbit anti-GFP polyclonal antibodies (Clontech) at 1/800. The secondary antibodies were Cy3-conjugated goat anti-mouse IgG antibodies (Jackson Immunoresearch) at 1/200, and FITC-conjugated goat anti-rabbit IgG (Sigma) at 1/200. In Fig. 4b, each bar represents a total of two independent experiments (number of animals scored; 10–20) for *let-60(*gf*)* and *let-60(*lf*)*, and three independent experiments ($n = 27$–67) for other strains.

Received 6 December 1999; accepted 20 January 2000.

1. Sternberg, P. W. & Han, M. Genetics of RAS signaling in *C. elegans*. *Trends Genet.* **14,** 466–472 (1998).
2. Bargmann, C. I., Hartwieg, E. & Horvitz, H. R. Odorant-selective genes and neurons mediate olfaction in *C. elegans*. *Cell* **74,** 515–527 (1993).
3. Beitel, G. J., Clark, S. G. & Horvitz, H. R. *Caenorhabditis elegans ras* gene *let-60* acts as a switch in the pathway of vulval induction. *Nature* **348,** 503–509 (1990).
4. Church, D. L., Guan, K. L. & Lambie, E. J. Three genes of the MAP kinase cascade, *mek-2*, *mpk-1/sur-1* and *let-60 ras*, are required for meiotic cell cycle progression in *Caenorhabditis elegans*. *Development* **121,** 2525–2535 (1995).
5. Kornfeld, K., Hom, D. B. & Horvitz, H. R. The *ksr-1* gene encodes a novel protein kinase involved in Ras-mediated signaling in *C. elegans*. *Cell* **83,** 903–913 (1995).
6. Sundaram, M. & Han, M. The *C. elegans ksr-1* gene encodes a novel Raf-related kinase involved in Ras-mediated signal transduction. *Cell* **83,** 889–901 (1995).
7. Clark, S. G., Stern, M. J. & Horvitz, H. R. *C. elegans* cell-signalling gene *sem-5* encodes a protein with SH2 and SH3 domains. *Nature* **356,** 340–344 (1992).
8. Tan, P. B., Lackner, M. R. & Kim, S. K. MAP kinase signaling specificity mediated by the LIN-1 Ets/LIN-31 WH transcription factor complex during *C. elegans* vulval induction. *Cell* **93,** 569–580 (1998).
9. Yu, S., Avery, L., Baude, E. & Garbers, D. L. Guanylyl cyclase expression in specific sensory neurons: A new family of chemosensory receptors. *Proc. Natl Acad. Sci. USA* **94,** 3384–3387 (1997).
10. Coburn, C. M., Mori, I., Ohshima, Y. & Bargmann, C. I. A cyclic nucleotide-gated channel inhibits sensory axon outgrowth in larval and adult *Caenorhabditis elegans*: a distinct pathway for maintenance of sensory axon structure. *Development* **125,** 249–258 (1998).
11. Coburn, C. M. & Bargmann, C. I. A putative cyclic nucleotide-gated channel is required for sensory development and function in *C. elegans*. *Neuron* **17,** 695–706 (1996).
12. Peckol, E. L., Zellen, J. A., Yarrow, J. C. & Bargmann, C. I. Sensory activity affects sensory axon development in *C. elegans*. *Development* **126,** 1891–1902 (1999).
13. Troemel, E. R., Kimmel, B. E. & Bargmann, C. I. Reprogramming chemotaxis responses: sensory neurons define olfactory preferences in *C. elegans*. *Cell* **91,** 161–169 (1997).
14. Albertson, D. G. & Thomson, J. N. The pharynx of *Caenorhabditis elegans*. *Phil. Trans. R. Soc. Lond. B Biol. Sci.* **275,** 299–325 (1976).
15. Roayaie, K., Crump, J. G., Sagasti, A. & Bargmann, C. I. The G alpha protein ODR-3 mediates olfactory and nociceptive function and controls cilium morphogenesis in *C. elegans* olfactory neurons. *Neuron* **20,** 55–67 (1998).
16. Komatsu, H., Mori, I., Rhee, J. S., Akaike, N. & Ohshima, Y. Mutations in a cyclic nucleotide-gated channel lead to abnormal thermosensation and chemosensation in *C. elegans*. *Neuron* **17,** 707–718 (1996).
17. Schafer, W. R. & Kenyon, C. J. A calcium-channel homologue required for adaptation to dopamine and serotonin in *Caenorhabditis elegans*. *Nature* **375,** 73–78 (1995).
18. Schild, D. & Restrepo, D. Transduction mechanisms in vertebrate olfactory receptor cells. *Physiol. Rev.* **78,** 429–466 (1998).
19. Prasad, B. C. & Reed, R. R. Chemosensation: molecular mechanisms in worms and mammals. *Trends Genet.* **15,** 150–153 (1999).
20. Bargmann, C. I. Neurobiology of the *Caenorhabditis elegans* genome. *Science* **282**, 2028–2033 (1998).
21. Goodman, M. B., Hall, D. H., Avery, L. & Lockery, S. R. Active currents regulate sensitivity and dynamic range in *C. elegans* neurons. *Neuron* **20,** 763–772 (1998).
22. Finkbeiner, S. & Greenberg, M. E. Ca^{2+}-dependent routes to Ras: mechanisms for neuronal survival, differentiation, and plasticity? *Neuron* **16,** 233–236 (1996).

23. Farnsworth, C. L. *et al.* Calcium activation of Ras mediated by neuronal exchange factor Ras–GRF. *Nature* **376,** 524–527 (1995).
24. Brambilla, R. *et al.* A role for the Ras signalling pathway in synaptic transmission and long-term memory. *Nature* **390,** 281–286 (1997).
25. Dusenbery, D. B., Sheridan, R. E. & Russell, R. L. Chemotaxis-defective mutants of the nematode *Caenorhabditis elegans*. *Genetics* **80,** 297–309 (1975).
26. Bargmann, C. I. & Horvitz, H. R. Chemosensory neurons with overlapping functions direct chemotaxis to multiple chemicals in *C. elegans*. *Neuron* **7,** 729–742 (1991).
27. Mello, C. C., Kramer, J. M., Stinchcomb, D. & Ambros, V. Efficient gene transfer in *C. elegans*: extra-chromosomal maintenance and integration of transforming sequences. *EMBO J.* **10,** 3959–3970 (1991).
28. Nonet, M. L. *et al.* *Caenorhabditis elegans rab-3* mutant synapses exhibit impaired function and are partially depleted of vesicles. *J. Neurosci.* **17,** 8061–8073 (1997).
29. Yung, Y. *et al.* Detection of ERK activation by a novel monoclonal antibody. *FEBS Lett.* **408,** 292–296 (1997).

Acknowledgements

We thank D. Garbers for the *gcy-10*::*GFP* reporter plasmid; M. Han for *let-60* cDNAs and the *mek-2(ku114)* strain; M. Koga, Y. Ohshima, N. Hisamoto and K. Matsumoto for pEF1α::GFP; A. Fire for vectors; and C. Bargmann, T. Schedl and Y. Emori for their comments and advice. All other nematode strains used in this study were provided by the Caenorhabditis Genetics Center, which is funded by the NIH National Center for Research Resources (NCRR).

Correspondence and requests for materials should be addressed to Y.I. (e-mail: iino@ims.u-tokyo.ac.jp).

An RNA-directed nuclease mediates post-transcriptional gene silencing in *Drosophila* cells

Scott M. Hammond*, Emily Bernstein†‡, David Beach*§ & Gregory J. Hannon‡

** Genetica, Inc., P.O. Box 99, Cold Spring Harbor, New York 11724, USA*
† Graduate Program in Genetics, State University of New York at Stony Brook, Stony Brook, New York 11794, USA
§ Wolfson Institute for Biological Sciences, University College London, Gower Street, London WC1E 6BT, UK
‡ Cold Spring Harbor Laboratory, 1 Bungtown Road, Cold Spring Harbor, New York 11724, USA

In a diverse group of organisms that includes *Caenorhabditis elegans*, *Drosophila*, planaria, hydra, trypanosomes, fungi and plants, the introduction of double-stranded RNAs inhibits gene expression in a sequence-specific manner[1–7]. These responses, called RNA interference or post-transcriptional gene silencing, may provide anti-viral defence, modulate transposition or regulate gene expression[1,6,8–10]. We have taken a biochemical approach towards elucidating the mechanisms underlying this genetic phenomenon. Here we show that 'loss-of-function' phenotypes can be created in cultured *Drosophila* cells by transfection with specific double-stranded RNAs. This coincides with a marked reduction in the level of cognate cellular messenger RNAs. Extracts of transfected cells contain a nuclease activity that specifically degrades exogenous transcripts homologous to transfected double-stranded RNA. This enzyme contains an essential RNA component. After partial purification, the sequence-specific nuclease co-fractionates with a discrete, ~25-nucleotide RNA species which may confer specificity to the enzyme through homology to the substrate mRNAs.

Although double-stranded RNAs (dsRNAs) can provoke gene silencing in numerous biological contexts including *Drosophila*[11,12], the mechanisms underlying this phenomenon have remained mostly unknown. We therefore wanted to establish a biochemically tractable model in which such mechanisms could be investigated.

Transient transfection of cultured, *Drosophila* S2 cells with a *lacZ* expression vector resulted in β-galactosidase activity that was easily detectable by an *in situ* assay (Fig. 1a). This activity was greatly reduced by co-transfection with a dsRNA corresponding to the first 300 nucleotides of the *lacZ* sequence, whereas co-transfection with a control dsRNA (*CD8*) (Fig. 1a) or with single-stranded RNAs of either sense or antisense orientation (data not shown) had little or no effect. This indicated that dsRNAs could interfere, in a sequence-specific fashion, with gene expression in cultured cells.

To determine whether RNA interference (RNAi) could be used to target endogenous genes, we transfected S2 cells with a dsRNA corresponding to the first 540 nucleotides of *Drosophila cyclin E*, a gene that is essential for progression into S phase of the cell cycle. During log-phase growth, untreated S2 cells reside primarily in G2/M (Fig. 1b). Transfection with *lacZ* dsRNA had no effect on cell-cycle distribution, but transfection with the *cyclin E* dsRNA caused a G1-phase cell-cycle arrest (Fig. 1b). The ability of *cyclin E* dsRNA to provoke this response was length-dependent. Double-stranded RNAs of 540 and 400 nucleotides were quite effective, whereas

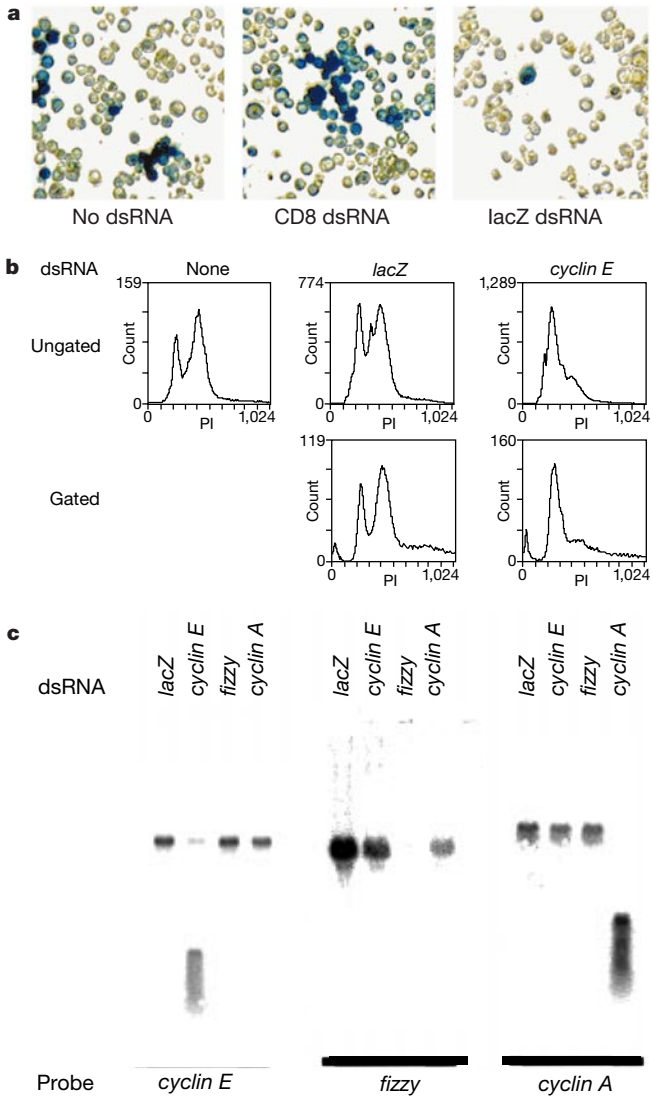

Figure 1 RNAi in S2 cells. **a**, *Drosophila* S2 cells were transfected with a plasmid that directs *lacZ* expression from the copia promoter in combination with dsRNAs corresponding to either human CD8 or lacZ, or with no dsRNA, as indicated. **b**, S2 cells were co-transfected with a plasmid that directs expression of a GFP–US9 fusion protein (12) and dsRNAs of either *lacZ* or *cyclin E*, as indicated. Upper panels show FACS profiles of the bulk population. Lower panels show FACS profiles from GFP-positive cells. **c**, Total RNA was extracted from cells transfected with *lacZ*, *cyclin E*, *fizzy* or *cyclin A* dsRNAs, as indicated. Northern blots were hybridized with sequences not present in the transfected dsRNAs.